ACT Publication No. 11-04

Mapping Impervious Surface Distribution with the Integration of Landsat TM and QuickBird Images in a Complex Urban–Rural Frontier in Brazil

Dengsheng Lu, Emilio Moran,
Scott Hetrick, and Guiying Li

In: Advances of Environmental Remote Sensing to Monitor Global Changes. Ni-Bin Chang (ed.), CRC Press/Taylor and Francis, pp. 277-296.

Anthropological Center for Training and Research on Global Environmental Change
Indiana University, Student Building 331, 701 E. Kirkwood Ave., 47405-7100, U.S.A.
Phone: (812) 855-6181, Fax: (812) 855-3000, Email: act@indiana.edu, internet: www.indiana.edu/~act

13 Mapping Impervious Surface Distribution with the Integration of Landsat TM and QuickBird Images in a Complex Urban–Rural Frontier in Brazil

Dengsheng Lu, Emilio Moran, Scott Hetrick, and Guiying Li

CONTENTS

13.1 INTRODUCTION

Impervious surfaces are generally defined as any man-made materials that water cannot infiltrate. They are primarily associated with human activities and habitation through the construction of transportation infrastructure and buildings (Slonecker et al. 2001; Bauer et al. 2008). Impervious surface area (ISA) has long been recognized as an important factor in many urban or environment related studies, including the improvement of urban land use and land cover (LULC) classification (Madhavan et al. 2001; Phinn et al. 2002; Lu and Weng 2006a), residential population estimation (Wu and Murray 2005; Lu et al. 2006), urban land use planning (Harbor 1994; Brabec et al. 2002), and urban environmental assessment, especially water quality (Schueler 1994; Arnold and Gibbons 1996; Zug et al. 1999; Brabec et al. 2002) and rainfall runoff (Lohani et al. 2002). Therefore, the timely and accurately mapping ISA distribution is of importance. The unique characteristics of remote sensing data in repetitive data acquisition, its synoptic view, and digital format suitable for computer processing make it the primary data source for ISA mapping. The research for extracting ISA from remotely sensed data has attracted great attention since the 1970s, especially in the most recent decade (Phinn et al. 2002; Gillies et al. 2003; Wu and Murray 2003; Yang et al. 2003a; Lu and Weng 2006a; Bauer et al. 2008; Mohapatra and Wu 2008; Wang et al. 2008; Xian et al. 2008; Hu and Weng 2009; Wu 2009; Weng et al., 2009; Yang et al. 2010). Since many new techniques for ISA mapping have been developed in recent decades, it is necessary to overview recent progress in order to provide guidelines for selecting a suitable technique for a specific study. This chapter briefly summarizes the major ISA mapping techniques that have appeared in recent literature and then provides a case study of ISA mapping with the integrated use of Landsat Thematic Mapper (TM) and QuickBird images in a complex urban–rural frontier in Brazil.

13.2 BACKGROUND

Urban landscapes can be regarded as a complex combination of buildings, roads, grass, trees, soil, water, and so on. In high spatial resolution images such as QuickBird and IKONOS, individual objects such as buildings and roads can be clearly identified; however, these features are less distinct in Landsat TM color composites because of Landsat's relatively coarse spatial resolution (i.e., 30 m; see Figure 13.1). Different construction materials often result in high spectral variation, that is, different ISA appears complex colors in QuickBird image, making it difficult to automatically map ISA distribution based on spectral signatures. In coarse and medium spatial resolution images such as Landsat TM, mixed pixels can be a serious problem, diminishing the effective use of remotely sensed data in urban LULC classification and change detection. If per-pixel based methods are used for mapping urban LULC distribution based on medium or coarse spatial resolution images, large uncertainty may be introduced into the result, that is, urban ISA extent could be significantly overestimated, and ISA in rural areas could be significantly underestimated (Lu and Weng 2004). This situation worsens if multitemporal remote sensing data are used for urban LULC change detection, especially in the urban–rural frontiers.

"appears as complex colors" meant?

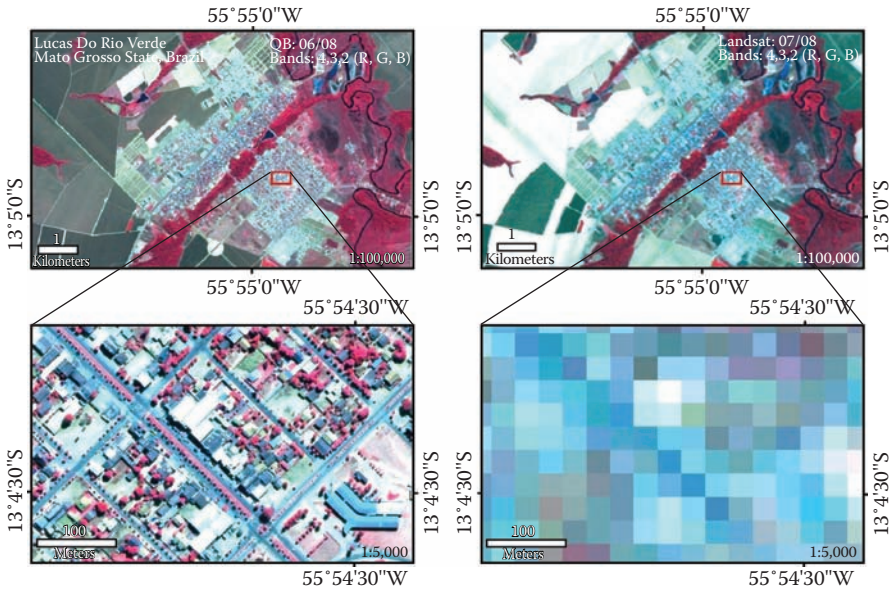

FIGURE 13.1 Comparison of color composites between QuickBird (left) and TM images (right), illustrating the mixed pixel problem in relatively coarse spatial resolution image.

In urban environments, land covers are assumed to be a linear combination of three components: vegetation, ISA, and soil (V-I-S) (Ridd 1995). The V-I-S model provides a guideline for decomposing urban landscapes and a link for these components to remote sensing spectral characteristics. Several studies have adopted this model as a basis for understanding the urban environment (Ward et al. 2000; Madhavan et al. 2001; Rashed et al. 2001; Phinn et al. 2002). From the view of remote sensing data, shade is also an important part affecting the spectral signature. Therefore, shade, green vegetation, soil, and ISA can almost explain all land covers in urban landscape (Lu and Weng 2004). In practice, ISA has high spectral variation; for example, bright building roofs may have very high spectral signatures that are confused with soils; dark roads and building roofs have very low spectral signatures that are often confused with shadow, water, and wetland (see Figure 13.1). Thus, direct extraction of ISA from remotely sensed data becomes very difficult because of the spectral confusion between ISA and other land covers. We can assume that urban landscape is composed of four components: high-albedo land covers, low-albedo land covers, vegetation, and soil. All land covers are a composition of these four components with linear or nonlinear relationship. Previous research has indicated that these four fraction images can be developed with spectral mixture analysis (Wu and Murray 2003; Lu and Weng 2006a,b). High-albedo fraction image highlights the land covers with high spectral reflectance, such as bright ISA and dry bare soils; low-albedo fraction image highlights the land cover with low spectral reflectance, such as dark ISA, shadow, water, and wetland. Soil fraction image highlights soil information, mainly located in agricultural lands; vegetation fraction image highlights the

OK to match with sentence below?

forest and plantation information. ISA is mainly concentrated on the high- and low-albedo fraction images; thus, ISA can be extracted from the addition of high- and low-albedo fraction images (Wu and Murray 2003; Lu and Weng 2006a,b).

Since the 1970s, many approaches for ISA mapping have been developed. Based on the achievements in the 1970s and 1980s, Slonecker et al. (2001) reviewed many of the approaches for ISA extraction from remotely sensed data and grouped them into three basic categories: interpretive applications, spectral applications, and modeling applications. Brabec et al. (2002) summarized four ways for ISA mapping: (1) using a planimeter to measure ISA on aerial photography, (2) counting the number of intersections on the overlain grid on an aerial photography, (3) conducting image classification, and (4) estimating ISA through the percentage of urbanization in a region. Recently, more advanced algorithms have been developed for quantitative extraction of ISA from satellite imagery. The major methods include per-pixel image classification (Lu and Weng 2009), subpixel classification (Ji and Jensen 1999; Phinn et al. 2002; Rashed et al. 2003), neural network (Mohapatra and Wu 2008; Wang et al. 2008; Hu and Weng 2009; Wu 2009), regression tree model (Yang et al. 2003a,b; Xian and Crane 2005; Xian 2008; Xian et al. 2008; Yang et al. 2009), the combination of high-albedo and low-albedo fraction images (Wu and Murray 2003; Wu 2004; Lu and Weng 2006a,b; Weng et al. 2008, 2009), and through the established relationship between ISA and vegetation cover (Gillies et al. 2003; Bauer et al. 2008). Major ISA mapping approaches can be summarized based on satellite images, which have appeared in recent literature (Table 13.1).

Image classification-based methods for mapping ISA are common (Slonecker et al. 2001; Brabec et al. 2002), but overestimation often occurs in urban extent and underestimation occurs in rural landscapes due to the limitation of spatial resolution in remotely sensed data and the heterogeneity in the urban environment (Lu and Weng 2004). The high spectral variation in ISA and similar spectral signatures between ISA and other nonvegetation land covers also make it difficult to select suitable training samples for the ISA class, resulting in misclassification. An alternative is to use ERDAS IMAGINE's subpixel classifier (Ji and Jensen 1999; Civco et al. 2002). However, the complexity of ISA materials often makes the subpixel classifier difficult to employ and leads to underestimation in ISA extraction. Since a high inverse correlation exists between vegetation cover and ISA in urban landscapes, the ISA can be estimated based on the established regression models with the vegetation indices, such as from tasseled cap greenness (Bauer et al. 2008) and fractional vegetation cover from the normalized difference vegetation index (NDVI) (Gillies et al. 2003). This approach has a drawback in that vegetation greenness varies with different seasons, which may result in large uncertainties of ISA estimation. Also this method cannot be directly transferred to other study areas or other dates of data sets due to local specificities regarding phenologies, climate conditions, and different composition of land covers in the urban landscape. Another common method for ISA estimation is based on the regression tree model (Yang et al. 2003a,b; Xian and Crane 2005; Xian 2008; Xian et al. 2008; Yang et al. 2009), which has been used for ISA mapping for continental United States based on Landsat TM images.

In recent years, spectral mixture analysis (SMA) has emerged as an important approach for ISA extraction from multispectral data. For example, ISA as one of the endmembers may be directly extracted from remotely sensed data (Rashed et al.

TABLE 13.1
Summary of Major Approaches for Impervious Surface Mapping

Category	Approach	Materials	References
Per-pixel based methods	Decision tree classifier, maximum likelihood	IKONOS, QuickBird	Goetz et al. 2003; Lu and Weng 2009; Lu et al. 2011
Subpixel based methods	Subpixel classifier	TM	Ji and Jensen, 1999
	Artificial neural networks	ASTER	Hu and Weng, 2009
	Subpixel proportional land cover information transformation (SPLIT)	TM, videography	Wang and Zhang, 2004
	Standard SMA	IRS-1C; TM	Rashed et al., 2001; Phinn et al., 2002
	Addition of low- and high-albedo fractions derived from standard or normalized SMA	ETM+	Wu and Murray, 2003; Wu, 2004
	Modified approach based on low-albedo, high-albedo, and land surface temperature	ETM+	Lu and Weng, 2006a, b
	Multiple endmember SMA	TM	Rashed et al., 2003
	Combination of support vector machines and geospatial analysis	ETM+, ATKIS vector data	Esch et al., 2009
	Regression tree model	ETM+	Xian and Crane 2005; Yang et al., 2003a, b
	Multiple regression analysis	DMSP-OLS, ancillary data	Elvidge et al., 2007; Sutton et al., 2009
Vegetation-based methods	A regression model based on impervious surface and tasseled cap greenness	TM	Bauer et al., 2008
	Based on fraction vegetation cover (Fr), i.e., 1-Fr for the developed areas	MSS and TM	Gillies et al., 2003
Other methods	A combination of image processing methods based on PCA and spatial morphological operators	IKONOS	Cablk and Minor, 2003
	Combination of knowledge-based classification and spectral unmixing	MSS/TM/ ETM+	Powell et al., 2008

2001; Phinn et al. 2002). ISA estimation may be improved by the addition of high- and low-albedo fraction images, which both are used as endmembers in SMA (Wu and Murray 2003; Lu and Weng 2006a,b). In addition, multiple endmember SMA (MESMA) (Rashed et al. 2003) has also been applied in which several ISA endmembers can be extracted. However, ISA is often overestimated or underestimated when medium spatial resolution images are used, depending on the relative proportion of

ISA in a pixel (Wu and Murray 2003; Lu and Weng 2006a,b; Greenfield et al. 2009). Since high spatial resolution satellite images (e.g., IKONOS and QuickBird) have become available, more research has shifted to the use of these data (Mohapatra and Wu 2008; Lu and Weng 2009; Wu 2009; Lu et al. 2011). However, the use of high spatial resolution images also presents a challenge for automatically mapping ISA distribution (Lu and Weng 2009). The main problems include spectral confusion between ISA and other land covers due to limited spectral resolution [i.e., usually only visible and near-infrared (NIR) wavelengths are available in very high spatial resolution images], high spectral variation within the same land cover, and shadows caused by tall objects and the confusion between dark ISA and water/wetland (Dare 2005; Li et al. 2005; Chen et al. 2007; Zhou et al. 2009).

13.3 RESEARCH PROBLEMS AND OBJECTIVES

In a complex urban–rural landscape, traditional classification methods cannot effectively distinguish ISA from other land covers due to the spectral confusion between dark ISA and wetland/water. A similar issue happens among bright ISA, soils, and cropped fields. Sometimes, traditional classification methods cannot effectively distinguish ISA from other land covers due to the difficulty in selecting training sample plots. Although subpixel-based methods can improve area estimation accuracy, it is critical and often difficult to distinguish the pixels with ISA from other land covers. Rarely has research focused on the improvement of ISA estimation in a complex urban–rural environment with multiscale remote sensing data. Therefore, this case study attempts to develop a new method suitable for a complex urban–rural landscape for mapping ISA distribution with the combination of Landsat TM and QuickBird images.

13.4 DESCRIPTION OF THE STUDY AREA

The city of Lucas do Rio Verde (hereafter called Lucas) in Mato Grosso State, Brazil, has a relatively short history and small urban extent (see Figure 13.2). It was established in 1982 and has experienced rapid urbanization. Highway BR 163 connects Lucas in the north to Santarém, a river port city on the Amazon River, and in the south to the heart of the soybean growing area at Cuiabá, capital city of Mato Grosso state. Highway BR-163 is a major route for the transport of export bound commodities grown in the region. The economic base of Lucas is large-scale agriculture, including the production of soy, cotton, rice, and corn as well as poultry and swine, to take advantage of the grain feed to add value to production. Major poultry and meat producing industries are developing as are other industrial complexes to add value to the agricultural output, which is now substantial. The county is at the epicenter of soybean production in Brazil, and it is expected to grow in population threefold in the next 10 years (personal communication with secretariat for planning at Lucas). Because this relatively small town has complex urban–rural spatial patterns derived from its highly capitalized agricultural base, large silos and warehouses, and planned urban growth, Lucas is an ideal site for exploring the methods for rapidly mapping urban extent with remotely sensed data.

Is year or name needed?

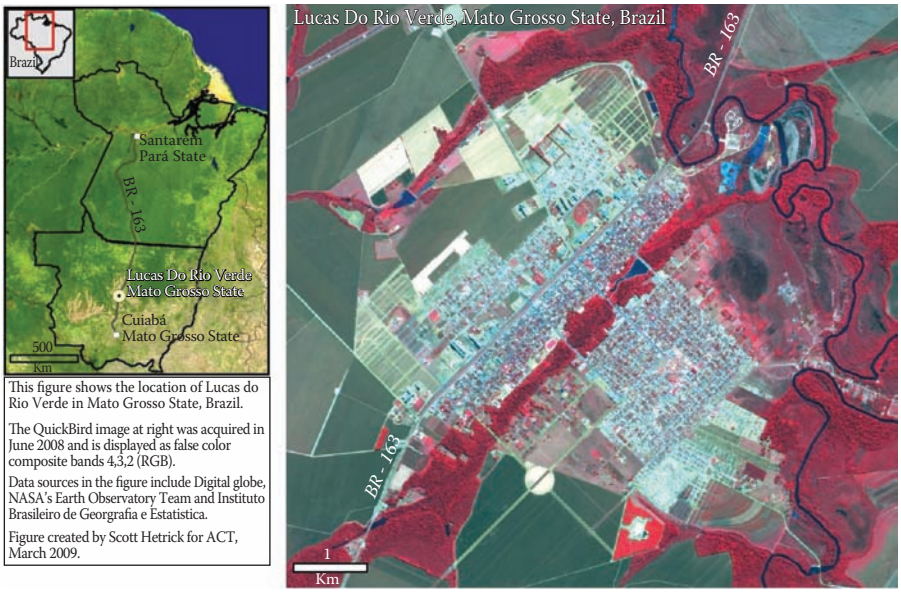

Is "false color composite bands" ok?

FIGURE 13.2 Study area, Lucas do Rio Municipio, Mato Grosso State, Brazil.

13.5 METHODOLOGY

Mapping ISA with Landsat images in a complex urban–rural frontier is challenging due to the mixed pixel problem and the confusion of ISA with other land covers. This research designed a comprehensive method based on the combined use of QuickBird and Landsat images, as illustrated in Figure 13.3. The major steps include: (1) mapping ISA with a hybrid method based on QuickBird imagery, (2) extracting per-pixel ISA images from Landsat images based on the thresholding of maximum and minimum filtering images and unsupervised classification, (3) mapping fractional images of high-albedo, low-albedo, vegetation, and soil endmembers with linear spectral

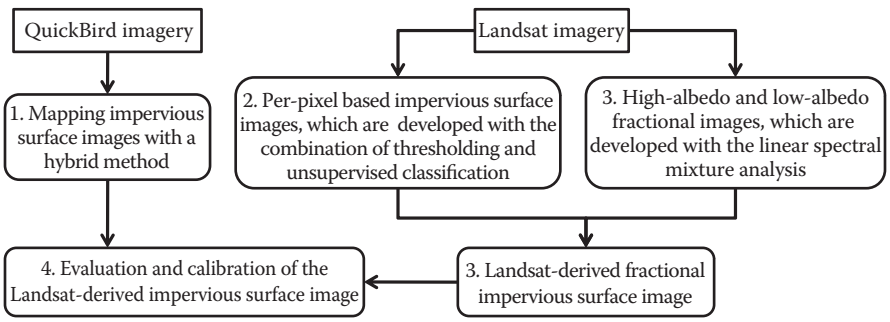

FIGURE 13.3 Strategy of integrating Landsat TM and QuickBird images for mapping impervious surface distribution.

mixture analysis (LSMA), and producing a fractional ISA image by adding high-albedo and low-albedo fraction images while removing non-ISA pixels by combining the per-pixel ISA image from step 2, and (4) establishing a regression model to calibrate the Landsat-derived ISA by using the QuickBird-derived ISA imagery.

13.5.1 Image Preprocessing

A Landsat TM image acquired on May 22, 2008 and a QuickBird image acquired on June 20, 2008 were used in this research. The TM image was geometrically registered into a Universal Transverse Mercator (UTM) projection with geometric error of less than 0.5 pixel. The nearest neighbor resampling method was used to resample the Landsat image into a pixel size of 30 m by 30 m during image-to-image registration. Radiometric and atmospheric correction was conducted on the TM image by utilizing the dark object subtraction (DOS) approach. The DOS model is an image-based procedure that standardizes imagery for the effects caused by solar zenith angle, solar radiance, and atmospheric scattering (Lu et al. 2002; Chander et al. 2009). Here are the equations used for Landsat image calibration:

$$R_\lambda = PI \cdot D \cdot (L_\lambda - L_{\lambda haze})/(Esun_\lambda \cdot COS\,(\theta)) \tag{13.1}$$

$$L_\lambda = gain_\lambda \cdot DN_\lambda + bias_\lambda \tag{13.2}$$

where L_λ is the apparent at-satellite radiance for spectral band λ, DN_λ is the digital number of spectral band λ, R_λ is the calibrated reflectance, $L_{\lambda.haze}$ is path radiance, $Esun_\lambda$ is exoatmospheric solar irradiance, D is the distance between the Earth and Sun, and θ is the Sun zenith angle. The path radiance for each band is identified based on the analysis of water bodies and shades in the images. The $gain_\lambda$ and $bias_\lambda$ are radiometric gain and bias corresponding to spectral band λ, respectively, and they are often provided in an image head file or metadata file, or calculated from maximal and minimal spectral radiance values (Lu et al. 2002).

13.5.2 Mapping ISA with QuickBird Imagery

QuickBird imagery is used to develop ISA data that is used as a reference for establishing a calibration model for refining the Landsat-derived ISA image. QuickBird imagery has four multispectral bands with 2.4-m spatial resolution and one panchromatic band with 0.6-m spatial resolution. In order to make full use of both the multispectral and panchromatic images, the wavelet merging technique (Lu et al. 2008) was used to merge the QuickBird multispectral bands and panchromatic band into a new multispectral image with 0.6-m spatial resolution. A hybrid method that consisted of thresholding, unsupervised classification, and manual editing was used to produce the ISA image from the fused QuickBird imagery (Lu et al. 2011) (see Figure 13.4). The fact that vegetation has significantly different spectral features comparing with ISA in the NDVI image and clear and deep water bodies have much lower spectral values than ISA in the NIR wavelength image, the vegetation and

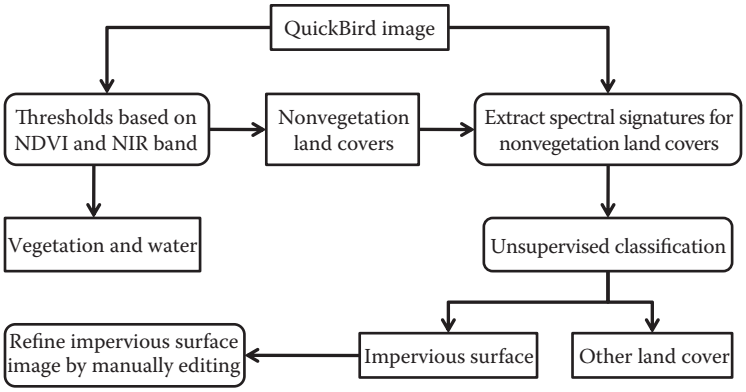

FIGURE 13.4 Framework of impervious surface mapping with the hybrid method.

water pixels can be masked out with selected thresholds on NDVI and NIR images. The major steps for the hybrid approach include (1) producing the NDVI image from QuickBird red and near-infrared images and then masking vegetation out with the selected threshold on the NDVI image, and masking water out with the selected thresholds on the NIR image, (2) extracting spectral signatures of the nonvegetation pixels, using an unsupervised classification algorithm to classify the extracted spectral signatures into 50 clusters and merging the clusters into ISA and other classes, and (3) manually editing the extracted ISA image (Lu et al. 2011). Although unsupervised classification can separate most ISA from bare soils and wetlands, some confusion still remains between bare soil and bright ISA, and among dark ISA, shadowed ISA, wetlands, or shadows from tree crowns. Therefore, visually interpreting the extracted ISA image is necessary to further refine the ISA image quality by eliminating the confused pixels (e.g., bare soils, non-ISA shadows, and wetlands).

Accuracy assessment is conducted with the error matrix approach (Congalton and Mead 1983; Congalton 1991; Janssen and van der Wel 1994; Foody 2002; Congalton and Green 2008). A total of 450 test samples were selected with the random sampling method. The analyst then examined each test sample plot to decide whether it was correctly classified as ISA or not based on visual interpretation on the QuickBird color composite. When the accuracy is satisfied, the ISA image with spatial resolution of 0.6 m is finally aggregated to 30 m to generate fractional ISA image for use as reference data.

13.5.3 Developing Per-Pixel Based ISA from Landsat Images

Per-pixel ISA mapping is often based on the image classification of spectral signatures (Shaban and Dikshit 2001; Lu et al. 2011), but per-pixel based classification methods based on medium or coarse spatial resolution images cannot effectively extract the ISA because of the spectral confusion between ISA and other land covers and the mixed pixel problems, especially in a complex urban–rural frontier (Wu and Murray 2003; Lu and Weng 2006a). This research for mapping per-pixel ISA was based on

the combination of filtering images and unsupervised classification of Landsat spectral signatures. The fact that the red-band image in Landsat TM has high spectral values for ISA but has low spectral values for vegetations and water/wetlands provides a potential way to rapidly map ISA. The minimum and maximum filter with a window size of 3 × 3 pixels was separately applied to the Landsat red-band image. The image differencing between maximum and minimum filtering images was used to highlight linear features (mainly roads) and other ISAs. Examination of the difference image indicated that a threshold of 13 value can extract the ISA image. The spectral signature of the initial ISA image was then extracted and was further classified into 60 clusters using an unsupervised classification method to refine the ISA image by removing the non-ISA pixels. Finally, manual editing of the ISA image was conducted to make sure that all ISAs, especially in urban regions, were extracted. The final per-pixel based ISA image was overlain on the TM color composite to visually examine the ISA mapping quality in order to make sure all urban area and major roads were properly extracted.

Should this be changed to "threshold value of 13"?

13.5.4 Mapping Fractional ISA Distribution

As per-pixel methods based on medium or coarse spatial resolution often overestimate or underestimate ISA, it is important to estimate fractional ISA images in order to improve area estimation. Of the many methods for mapping ISA (Slonecker et al. 2001; Brabec et al. 2002), the LSMA-based method has proven valuable for extracting fractional ISA from Landsat images (Wu and Murray 2003; Lu and Weng 2006a,b). LSMA is regarded as a physically based image-processing tool. It supports repeatable and accurate extraction of quantitative subpixel information (Smith et al. 1990). The LSMA approach assumes that the spectrum measured by a sensor is a linear combination of the spectra of all components (endmembers) within the pixel and that the spectral proportions of the endmembers represent proportions of the area covered by distinct features on the ground (Adams et al. 1995; Mustard and Sunshine 1999). The mathematical model can be expressed as

$$R_i = \sum_{k=1}^{n} f_k R_{ik} + \varepsilon_i \tag{13.3}$$

where i is the number of spectral bands used; $k = 1, \ldots, n$ (number of endmembers), R_i is the spectral reflectance of band i of a pixel that contains one or more endmembers, f_k is the proportion of endmember k within the pixel, R_{ik} is known as the spectral reflectance of endmember k within the pixel on band i, and ε_i is the error for band i. For a constrained least squares solution, f_k is subject to the following restrictions:

$$\sum_{k=1}^{n} f_k = 1 \text{ and } 0 \le f_k \le 1 \tag{13.4}$$

$$\text{RMSE} = \sqrt{\left(\sum_{i=1}^{m} \varepsilon_i^2 / m\right)} \tag{13.5}$$

The root-mean-square error (RMSE) is used to assess the fit of the model. It is calculated for all image pixels. The larger the RMSE is, the worse the fit of the model is. So the error image can be used to assess whether the endmembers are properly selected and whether the number of selected endmembers is sufficient.

In the LSMA approach, endmember selection is a key step, and many approaches have been developed (Lu et al. 2003; Theseira et al. 2003). In practice, image-based endmember selection methods are frequently used because image endmembers can be easily obtained and they represent the spectra measured at the same scale as the image data. Image endmembers can be derived from the extremes of the image feature space, assuming that they represent the purest pixels in the images (Mustard and Sunshine 1999). In order to effectively identify image endmembers and to achieve high-quality endmembers, different image transform approaches such as principal component analysis (PCA) and minimum noise fraction (MNF) may be used to transform the multispectral images into a new data set (Green et al. 1988; Boardman and Kruse 1994). Endmembers are then selected from the feature spaces of the transformed images (Garcia-Haro et al. 1996; Cochrane and Souza 1998; van der Meer and de Jong 2000; Small 2001, 2002, 2004). In this research, four endmembers (i.e., high-albedo objects, low-albedo objects, vegetation, and soil) were selected from the feature spaces formed by the MNF components. A constrained least squares solution was then used to unmix the Landsat TM multispectral image into four fractional images and one error image.

Previous research indicates that the high-albedo fraction image contains the bright ISA objects such as building roofs with high spectral values, and low-albedo fraction image contains the dark ISA objects such as dark roads and streets with low spectral values (Lu and Weng 2006a,b). Therefore, the overall ISA image can be extracted from the addition of high-albedo and low-albedo fraction images. One critical step in mapping ISA is to remove the non-ISA pixels. The strategy of mapping fractional ISA can be illustrated based on the LSMA-based methods and per-pixel based method (Figure 13.5). By combining per-pixel ISA and high- and low-albedo fraction images, a fractional ISA image was then generated with the following rules: if the pixel is ISA in the per-pixel based ISA image, the pixel value is then extracted from the sum of high-albedo and low-albedo fraction images; otherwise, assign zero to the pixel.

13.5.5 Refining ISA by Integrated Use of Landsat- and QuickBird-derived ISA Images

Previous research also indicates that the developed ISA data set from Landsat TM images is often overestimated or underestimated, depending on the proportion of ISA in a pixel (Wu and Murray 2003; Lu and Weng 2006a). In the complex urban–rural landscape, ISA estimation with LSMA-based method often overestimates its area

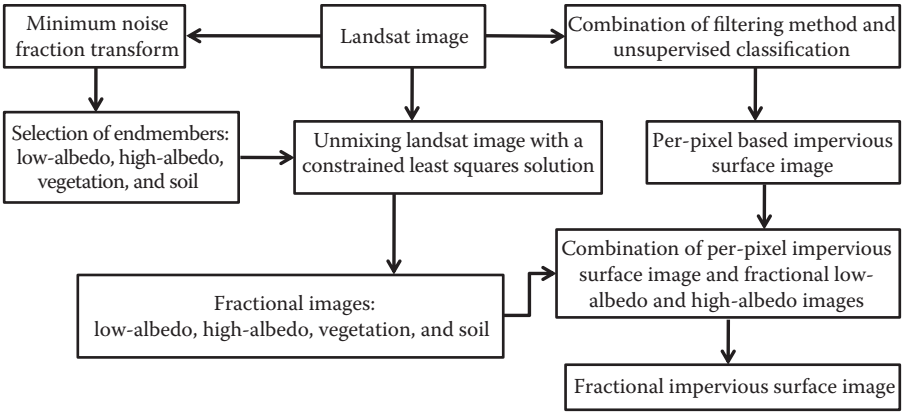

FIGURE 13.5 Strategy of developing fractional impervious surface images based on the combination of linear spectral mixture analysis and per-pixel based method.

statistics. It is necessary to calibrate this bias. One method is to develop a regression model to calibrate the TM-derived ISA images. In this research, the overlap area between the 2008 QuickBird and the corresponding Landsat-derived ISA images was used for sample collection based on this rule: select one pixel for every five intervals on the overlapped images. Because many pixels were non-ISA, they had zero values. After removal of all samples with zero values, 1512 samples were used to develop the calibration model. A scatterplot of these samples was used to examine the relationship between the Landsat-derived and QuickBird-derived ISA images. A regression model was developed to conduct the calibration.

13.6 RESULTS AND DISCUSSION

13.6.1 ISA Mapping with QuickBird Imagery

A high-quality ISA data set from QuickBird imagery is required because it is used as reference data for calibrating Landsat-derived ISA data set. The accuracy assessment based on randomly selected 450 sample plots indicated that 98% overall accuracy was achieved, according to visual interpretation on the QuickBird color composite. The spatial patterns of ISA distribution can be shown in Figure 13.6. The QuickBird-derived ISA data were then aggregated from 0.6 to 30 m cell sizes to generate fractional ISA data for use in linking it to Landsat TM image for calibration.

13.6.2 Evaluation of Per-Pixel ISA Image from Landsat TM Imagery

Evaluation of the per-pixel ISA image based on overlaying it on the TM color composite indicates that a combination of filtering images and unsupervised classification method developed in this research can effectively extract the pixel-based ISA data set in the complex urban–rural frontier. In per-pixel based results, each

FIGURE 13.6 Impervious surface image developed from QuickBird imagery.

extracted ISA pixel is assumed to be 100% ISA. This data set is useful for visually interpreting the ISA distribution, but not suitable for area statistics. Therefore, it is necessary to produce a subpixel ISA data set for area statistical purpose in order to remove the impact of the mixed pixel problem.

13.6.3 Development of Fractional ISA Image from Landsat TM Imagery

The four fraction images developed from Landsat TM imagery with the LSMA approach have physical meanings as described in Section 13.2. ISA is mainly concentrated on high-albedo and low-albedo fraction images; thus, the fractional ISA data can be directly extracted through the addition of the high-albedo and low-albedo fraction images. However, some roads appear in the soil fraction image due to the confusion of their spectral signatures (see Figure 13.7), and some non-ISA pixels, such as water, are also included in the initial fractional ISA image. Therefore, the per-pixel based ISA image is used to mask out the non-ISA pixels from the fractional ISA image. A comparison of per-pixel ISA can be summarized (Figure 13.8a and b). Fractional ISA (Figure 13.8c and d) images indicated that the area amount may be significantly overestimated by the per-pixel ISA image. Because of the limitation of the LSMA method in extracting ISA information from other land covers, underestimation or overestimation of ISA is common, as shown in previous research (Lu and

Please check if the changes made here are correct.

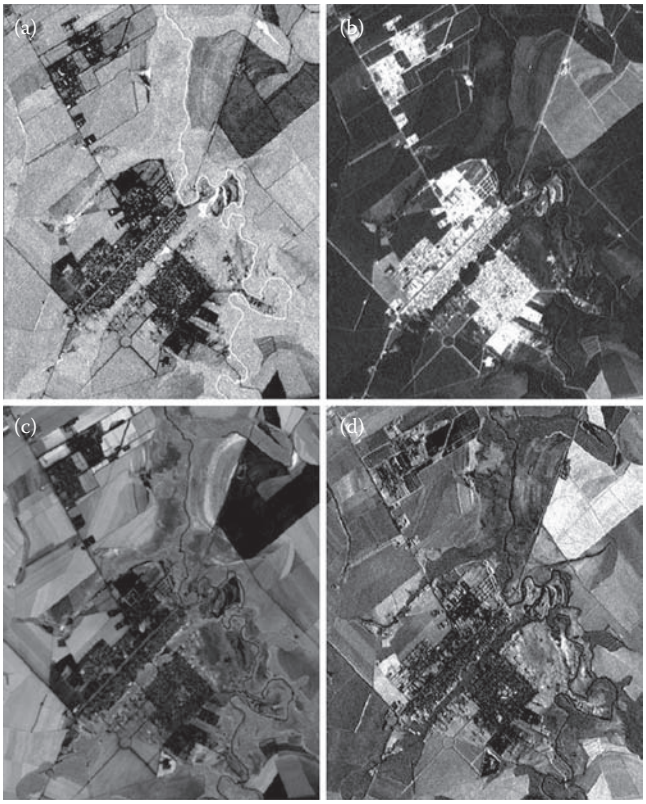

FIGURE 13.7 Fraction images developed with linear spectral mixture analysis based on Landsat TM multispectral data: (a) low-albedo, (b) high-albedo, (c) vegetation, and (d) soil.

Weng 2006a,b); thus, it is necessary to further calibrate the fractional ISA image to improve the area estimation accuracy.

13.6.4 Calibration of the Landsat-Derived Fractional ISA with the QuickBird-Derived ISA Image

In theory, if the ISA data are accurately estimated from both Landsat TM and QuickBird images, the scatterplot between both fractional ISA data sets should show a very good linear relationship. As shown in Figure 13.9, the ISA image developed in this research demonstrates a reasonably good result, although overestimation occurred when the ISA accounted for a relatively small proportion in a pixel and underestimation occurred when the ISA accounted for a large proportion in a pixel. This trend is similar in other previous research (Wu and Murray 2003; Lu and Weng 2006; Greenfield et al. 2009). Overall, a good linear relationship exists between the fractional ISA images developed independently from 2008 Landsat TM

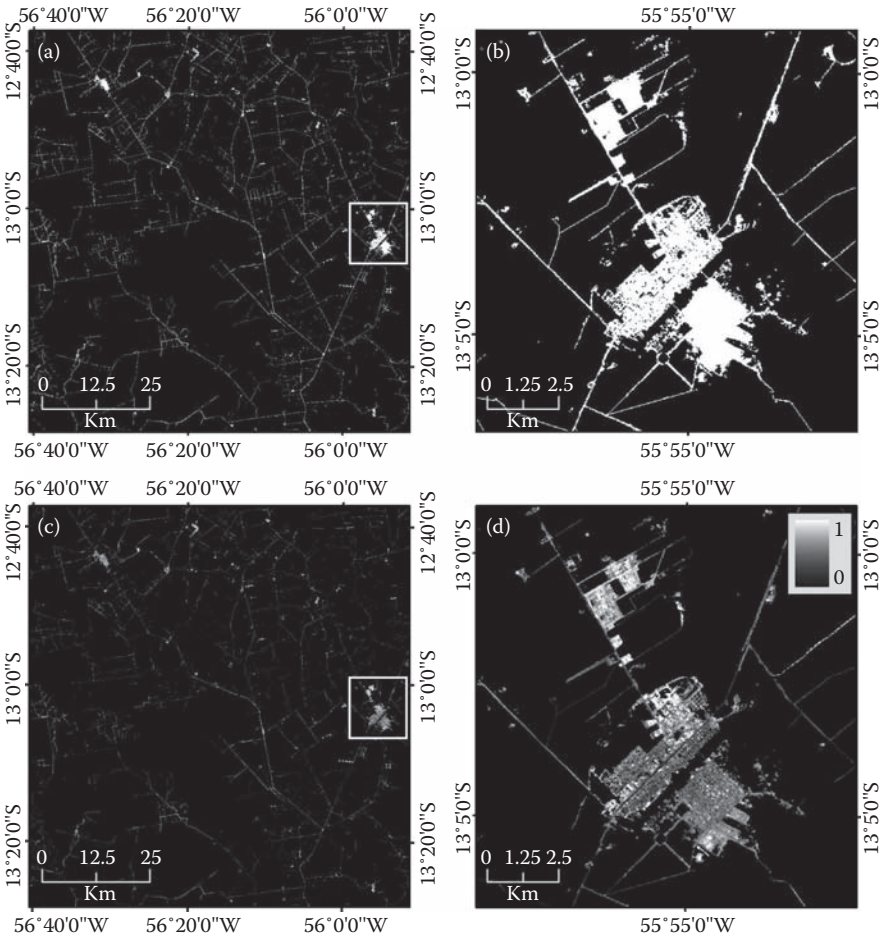

FIGURE 13.8 Comparison of impervious surface results with pixel-based (a and b) and subpixel-based (c and d) methods.

and QuickBird images. Based on the samples from QuickBird- and Landsat-derived ISA images, a linear regression model is established as follows:

Variables in italics (also in paragraph that follows)?

$$y = 1.0674x - 0.0119;\ R^2 = 0.45 \tag{13.6}$$

where x is the fractional ISA values from 2008 Landsat TM image, and y is the calibrated fraction ISA values. For the non-ISA pixels (i.e., x equals zero), assign a zero value to that pixel; otherwise, this equation was used to calibrate the entire image of 2008 Landsat TM-derived fractional ISA image. When the ISA was calculated from the per-pixel ISA image, the ISA for Lucas município (see Figure 13.2) was 99.87 km^2, accounting for 1.291% of the study area. However, when the ISA was calculated from the calibrated fractional ISA data set, the ISA became only 56.86 km^2,

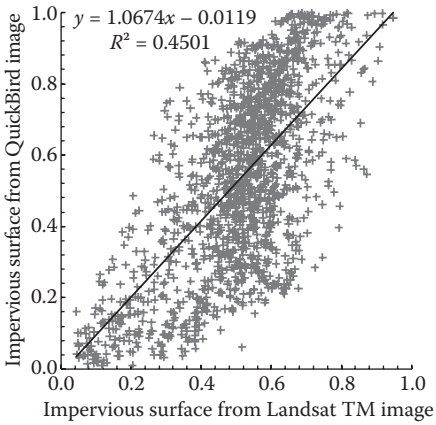

FIGURE 13.9 Relationship of fractional ISA data from Landsat TM and QuickBird images.

accounting for only 0.735%. This implies that development of fractional ISA data set is required for ISA measurement, especially in an urban–rural frontier.

13.7 CONCLUSIONS

The complexity of ISA in the urban landscape and the mixed pixel problem in medium and coarse spatial resolution images make the mapping of ISA a challenging task. Traditional per-pixel based image classification methods cannot effectively handle the mixed pixel problem, and subpixel-based methods cannot effectively separate the pixels of ISA from other land covers; thus, underestimation or overestimation of the ISA are common, depending on the proportion of ISA in a pixel. The method described in this chapter, which is based on the combination of per-pixel based ISA mapping with filtering and unsupervised classification, and subpixel-based method with the LSMA approach, can effectively map ISA distribution with Landsat images. The calibration with QuickBird-derived ISA data set can further reduce the bias caused by mixed pixel problems and thus improve ISA mapping performance. The major advantage of the method described in this chapter is that the ISA estimation can be considerably improved comparing with per-pixel based results in a complex urban–rural frontier. More research is needed to apply this method to other study areas and other dates of Landsat images to examine its transferability and robustness.

ACKNOWLEDGMENT

The authors wish to thank the National Institute of Child Health and Human Development at NIH (grant # R01 HD035811) for the support of this research, addressing population-and-environment reciprocal interactions, in several regions of the Brazilian Amazon. Any errors are solely the responsibility of the authors and not of the funding agencies.

REFERENCES

Adams, J. B., Sabol, D. E., Kapos, V., Filho, R. A., Roberts, D. A., Smith, M. O., and Gillespie, A. R. (1995). Classification of multispectral images based on fractions of endmembers: Application to land cover change in the Brazilian Amazon. *Remote Sensing of Environment*, 52, 137–154.

Arnold, C. L. and Gibbons, C. J. (1996). Imperious surface coverage: the emergence of a key environmental indicator. *Journal of the American Planning Association*, 62(2), 243–258.

Bauer, M. E., Loffelholz, B. C., and Wilson, B. (2008). Estimating and mapping impervious surface area by regression analysis of Landsat imagery. In *Remote Sensing of Impervious Surfaces,* Q. Weng (ed.), Taylor & Francis Group, LLC, Boca Raton, FL, pp. 3–19.

Boardman, J. W. and Kruse, F. A. (1994). Automated spectral analysis: A geological example using AVIRIS data, North Grapevine Mountains, Nevada. In *Proceedings, ERIM Tenth Thematic Conference on Geologic Remote Sensing*, Ann Arbor, MI, pp. 407–418.

Brabec, E., Schulte, S., and Richards, P. L. (2002). Impervious surface and water quality: A review of current literature and its implications for watershed planning. *Journal of Planning Literature*, 16, 499–514.

Cablk, M. E. and Minor, T. B. (2003). Detecting and discriminating impervious cover with high-resolution IKONOS data using principal component analysis and morphological operators. *International Journal of Remote Sensing*, 24, 4627–4645.

Chander, G., Markham, B. L., and Helder, D. L. (2009). Summary of current radiometric calibration coefficients for Landsat MSS, TM, ETM+, and EO-1 ALI sensors. *Remote Sensing of Environment*, 113, 893–903.

Chen, Y., Wen, D., Jing, L., and Shi, P. (2007). Shadow information recovery in urban areas from very high resolution satellite imagery. *International Journal of Remote Sensing,* 28, 3249–3254.

Civco, D. L., Hurd, J. D., Wilson, E. H., Arnold, C. L., and Prisloe Jr., M. P. (2002). Quantifying and describing urbanizing landscapes in the northeast United States. *Photogrammetric Engineering and Remote Sensing*, 68, 1083–1090.

Cochrane, M. A. and Souza, C. M. Jr. (1998). Linear mixture model classification of burned forests in the eastern Amazon. *International Journal of Remote Sensing,* 19, 3433–3440.

Congalton, R. G. (1991). A review of assessing the accuracy of classification of remotely sensed data. *Remote Sensing of Environment*, 37, 35–46.

Congalton, R. G. and Mead, R. A. (1983). A quantitative method to test for consistency and correctness in photo interpretation. *Photogrammetric Engineering and Remote Sensing*, 49, 69–74.

Congalton, R. G. and Green, K. (2008). *Assessing the Accuracy of Remotely Sensed Data: Principles and Practices*, Second Edition, CRC Press, Taylor & Francis Group, Boca Raton, FL, p. 183.

Dare, P. M. (2005). Shadow analysis in high-resolution satellite imagery of urban areas. *Photogrammetric Engineering and Remote Sensing*, 71, 169–177.

Elvidge, C. D., Tuttle, B. T., Sutton, P. C., Baugh, K. E., Howard, A. T., Milesi, C., Bhaduri, B., and Nemani R. (2007). Global distribution and density of constructed impervious surfaces. *Sensors,* 7, 1962–1979.

Esch, T., Himmler, V., Schorcht, G., Thiel, M., Wehrmann, T., Bachofer, F., Conrad, C., Schmidt, M., and Dech, S. (2009). Large-area assessment of impervious surface based on integrated analysis of single-date Landsat-7 images and geospatial vector data. *Remote Sensing of Environment*, 113, 1678–1690.

Foody, G. M. (2002). Status of land cover classification accuracy assessment. *Remote Sensing of Environment*, 80, 185–201.

Garcia-Haro, F. J., Gilabert, M. A., and Melia, J. (1996). Linear spectral mixture modeling to estimate vegetation amount from optical spectral data. *International Journal of Remote Sensing*, 17, 3373–3400.

Goetz, S. J., Wright, R., Smith, A. J., Zinecker, E., and Schaub, E. (2003). IKONOS imagery for resource management: Tree cover, impervious surface, and riparian buffer analyses in the mid-Atlantic region. *Remote Sensing of Environment*, 88, 195–208.

Gillies, R. R., Box, J. B., Symanzik, J., and Rodemaker, E. J. (2003). Effects of urbanization on the aquatic fauna of the Line Creek watershed, Atlanta—A satellite perspective. *Remote Sensing of Environment*, 86, 411–422.

Green, A. A., Berman, M., Switzer, P., and Craig, M. D. (1988). A transformation for ordering multispectral data in terms of image quality with implications for noise removal. *IEEE Transactions on Geoscience and Remote Sensing*, 26, 65–74.

Greenfield, E. J., Nowak, D. J., and Walton, J. T. (2009). Assessment of 2001 NLCD percent tree and impervious cover estimates. *Photogrammetric Engineering and Remote Sensing*, 75, 1279–1286.

Harbor, J. M. (1994). A practical method for estimating the impact of land use change on surface runoff, groundwater recharge and wetland hydrology. *American Planning Association*, 60, 95–108.

Hu, X. and Weng, Q. (2009). Estimating impervious surfaces from medium spatial resolution imagery using the self-organizing map and multi-layer perceptron neural networks. *Remote Sensing of Environment*, 113, 2089–2102.

Janssen, L. F. J. and van der Wel, F. J. M. (1994). Accuracy assessment of satellite derived land-cover data: a review. *Photogrammetric Engineering and Remote Sensing*, 60, 419–426.

Ji, M. and Jensen, J. R. (1999). Effectiveness of subpixel analysis in detecting and quantifying urban imperviousness from Landsat Thematic Mapper. *Geocarto International*, 14, 31–39.

Li, Y., Gong, P., and Sasagawa, T. (2005). Integrated shadow removal based on photogrammetry and image analysis. *International Journal of Remote Sensing*, 26, 3911–3929.

Lohani, V., Kibler, D. F., and Chanat, J. (2002). Constructing a problem solving environment tool for hydrologic assessment of land use change. *Journal of the American Water Resources Association*, 38, 439–452.

Lu, D., Mausel, P., Brondízio, E., and Moran, E. (2002). Assessment of atmospheric correction methods for Landsat TM data applicable to Amazon basin LBA research. *International Journal of Remote Sensing*, 23, 2651–2671.

Lu, D., Moran, E., and Batistella, M. (2003). Linear mixture model applied to Amazonian vegetation classification. *Remote Sensing of Environment*, 87, 456–469.

Lu, D. and Weng, Q. (2004). Spectral mixture analysis of the urban landscapes in Indianapolis with Landsat ETM+ imagery. *Photogrammetric Engineering and Remote Sensing*, 70, 1053–1062.

Lu, D. and Weng, Q. (2006a). Use of impervious surface in urban land use classification. *Remote Sensing of Environment*, 102, 146–160.

Lu, D. and Weng, Q. (2006b). Spectral mixture analysis of ASTER images for examining the relationship between urban thermal features and biophysical descriptors in Indianapolis, United States. *Remote Sensing of Environment*, 104(2), 157–167.

Lu, D., Weng, Q., and Li, G. (2006). Residential population estimation using a remote sensing derived impervious surface approach. *International Journal of Remote Sensing*, 27(16), 3553–3570.

Lu, D., Batistella, M., Moran, E., and de Miranda, E. E. (2008). A comparative study of Landsat TM and SPOT HRG images for vegetation classification in the Brazilian Amazon. *Photogrammetric Engineering and Remote Sensing*, 70, 311–321.

Lu, D. and Weng, Q. (2009). Extraction of urban impervious surface from an IKONOS image. *International Journal of Remote Sensing*, 30(5), 1297–1311.

Lu, D., Hetrick, S., and Moran, E. (2011). Impervious surface mapping with QuickBird imagery. *International Journal of Remote Sensing*, 32(9), 2519–2533.

Madhavan, B. B., Kubo, S., Kurisaki, N., and Sivakumar, T. V. L. N. (2001). Appraising the anatomy and spatial growth of the Bangkok Metropolitan area using a vegetation-impervious-soil model through remote sensing. *International Journal of Remote Sensing*, 22, 789–806.

Mohapatra, R. P. and Wu, C. (2008). Subpixel imperviousness estimation with IKONOS imagery: An artificial neural network approach. In *Remote Sensing of Impervious Surfaces,* Q. Weng (ed.), Taylor & Francis Group, LLC, Boca Raton, FL, pp. 21–37.

Mustard, J. F. and Sunshine, J. M. (1999). Spectral analysis for earth science: Investigations using remote sensing data. In *Remote Sensing for the Earth Sciences: Manual of Remote Sensing*, Third Edition, Volume 3, A. N. Rencz (ed.), John Wiley & Sons Inc., New York, pp. 251–307.

Phinn, S., Stanford, M., Scarth, P., Murray, A. T., and Shyy, P. T. (2002). Monitoring the composition of urban environments based on the vegetation-impervious surface–soil (VIS) model by subpixel analysis techniques. *International Journal of Remote Sensing,* 23, 4131–4153.

Powell, S. L., Cohen, W. B., Yang, Z., Pierce, J. D., and Alberti, M. (2008). Quantification of impervious surface in the Snohomish Water Resources Inventory Area of Western Washington from 1972–2006. *Remote Sensing of Environment*, 112, 1895–1908.

Rashed, T., Weeks, J. R., Gadalla, M. S., and Hill, A. G. (2001). Revealing the anatomy of cities through spectral mixture analysis of multispectral satellite imagery: A case study of the Greater Cairo region, Egypt. *Geocarto International*, 16, 5–15.

Rashed, T., Weeks, J. R., Roberts, D., Rogan, J., and Powell, R. (2003). Measuring the physical composition of urban morphology using multiple endmember spectral mixture models. *Photogrammetric Engineering and Remote Sensing*, 69, 1011–1020.

Ridd, M. K. (1995). Exploring a V-I-S (vegetation-impervious surface-soil) model for urban ecosystem analysis through remote sensing: Comparative anatomy for cities. *International Journal of Remote Sensing*, 16, 2165–2185.

Schueler, T. R. (1994). The importance of imperviousness. *Watershed Protection Techniques,* 1, 100–111.

Shaban, M. A. and Dikshit, O. (2001). Improvement of classification in urban areas by the use of textural features: The case study of Lucknow city, Uttar Pradesh. *International Journal of Remote Sensing*, 22, 565–593.

Slonecker, E. T., Jennings, D., and Garofalo, D. (2001). Remote sensing of impervious surface: A review. *Remote Sensing Reviews*, 20, 227–255.

Small, C. (2001). Estimation of urban vegetation abundance by spectral mixture analysis. *International Journal of Remote Sensing*, 22, 1305–1334.

Small, C. (2002). Multitemporal analysis of urban reflectance. *Remote Sensing of Environment*, 81, 427–442.

Small, C. (2004). The Landsat ETM+ spectral mixing space. *Remote Sensing of Environment*, 93, 1–17.

Smith, M. O., Ustin, S. L., Adams, J. B., and Gillespie, A. R. (1990). Vegetation in Deserts: I. A regional measure of abundance from multispectral images. *Remote Sensing of Environment*, 31, 1–26.

Sutton, P. C., Anderson, S. A., Elvidge, C. D., Tuttle, B. T., and Ghosh, T. (2009). Paving the planet: Impervious surface as proxy measure of the human ecological footprint. *Progress in Physical Geography*, 33, 510–527.

Theseira, M. A., Thomas, G., Taylor, J. C., Gemmell, F., and Varjo, J. (2003). Sensitivity of mixture modeling to endmember selection. *International Journal of Remote Sensing*, 24, 1559–1575.

Van der Meer, F. and de Jong, S. M. (2000). Improving the results of spectral unmixing of Landsat Thematic Mapper imagery by enhancing the orthogonality of end-members. *International Journal of Remote Sensing*, 21, 2781–2797.

Wang, Y. and Zhang, X. (2004). A SPLIT model for extraction of subpixel impervious surface information. *Photogrammetric Engineering and Remote Sensing*, 70, 821–828.

Wang, Y., Zhou, Y., and Zhang, X. (2008). The SPLIT and MASC models for extraction of impervious surface areas from multiple remote sensing data. In *Remote Sensing of Impervious Surfaces,* Q. Weng (ed.), Taylor & Francis Group, LLC, Boca Raton, FL, pp. 77–92.

Ward, D., Phinn, S. R., and Murray, A. L. (2000). Monitoring growth in rapidly urbanizing areas using remotely sensed data. *Professional Geographer*, 53, 371–386.

Weng, Q., Hu, X., and Lu, D. (2008). Extracting impervious surface from medium spatial resolution multispectral and hyperspectral imagery: A comparison. *International Journal of Remote Sensing*, 29, 3209–3232.

Weng, Q., Hu, X., and Liu, H. (2009). Estimating impervious surfaces using linear spectral mixture analysis with multitemporal ASTER images. *International Journal of Remote Sensing*, 30(18), 4807–4830.

Wu, C. and Murray, A. T. (2003). Estimating impervious surface distribution by spectral mixture analysis. *Remote Sensing of Environment*, 84, 493–505.

Wu, C. (2004). Normalized spectral mixture analysis for monitoring urban composition using ETM+ imagery. *Remote Sensing of Environment*, 93, 480–492.

Wu, C. and Murray, A. T. (2005). A cokriging method for estimating population density in urban areas. *Computers, Environment and Urban Systems*, 29, 558–579.

Wu, C. (2009). Quantifying high-resolution impervious surfaces using spectral mixture analysis. *International Journal of Remote Sensing*, 30(11), 2915–2932.

Xian, G. and Crane, M. (2005). Assessments of urban growth in the Tampa Bay watershed using remote sensing data. *Remote Sensing of Environment*, 97, 203–215.

Xian, G. (2008). Mapping impervious surfaces using classification and regression tree algorithm. In *Remote Sensing of Impervious Surfaces*, Q. Weng (ed.), Taylor & Francis Group, LLC, Boca Raton, FL, pp. 39–58.

Xian, G., Crane, M. P., and McMahon, C. (2008). Quantifying multitemporal urban development characteristics in Las Vegas from Landsat and Aster data. *Photogrammetric Engineering and Remote Sensing*, 74, 473–481.

Yang, L., Xian, G., Klaver, J. M., and Deal, B. (2003a). Urban land-cover change detection through sub-pixel imperviousness mapping using remotely sensed data. *Photogrammetric Engineering and Remote Sensing*, 69, 1003–1010.

Yang, L., Huang, C., Homer, C., Wylie, B., and Coan, M. (2003b). An approach for mapping large-area impervious surface: synergistic use of Landsat 7 ETM+ and high spatial resolution imagery. *Canadian Journal of Remote Sensing*, 29, 230–240.

Yang, L., Jiang, L., Lin, H., and Liao, M. (2009). Quantifying sub-pixel urban impervious surface through fusion of optical and InSAR imagery. *GIScience and Remote Sensing*, 46(2), 161–171.

Yang, F., Matsushita, B., and Fukushima, T. (2010). A pre-screened and normalized multiple endmember spectral mixture analysis for mapping impervious surface area in Lake Kasumigaura Basin, Japan. *ISPRS Journal of Photogrammetry and Remote Sensing*, 65, 479–490.

Zhou, W., Huang, G., Troy, A., and Cadenasso, M. L. (2009). Object-based land cover classification of shaded areas in high spatial resolution imagery of urban areas: A comparison study. *Remote Sensing of Environment*, 113, 1769–1777.

Zug, M., Phan, L., Bellefleur, D., and Scrivener, O. (1999). Pollution wash-off modeling on impervious surface: Calibration, validation, and transposition. *Water Science and Technology*, 39, 17–24.

2010

No. 10-03
Lu, D., S. Hetrick, and E. Moran 2010. Land Cover Classification in a Complex Urban-rural Landscape with QuickBird Imagery. Photogrammetric Engineering & Remote Sensing 76(10):1159-1168.

No. 10-04
Lu, D., E. Moran, S. Hetrick and G. Li. In Press. Mapping Impervious Surface Distribution with the Integration of Landsat TM and Quickbird Images in a Complex Urban-rural Frontier in Brazil. Chapter 16.

No. 10-05
Lu, D., S. Hetrick, and E. Moran. In Press. Impervious Surface Mapping with Quickbird Imagery. International Journal of Remote Sensing.

No. 10-06
Mattos, L. and A. Cau. In Press. The Clean Development Mechanism and Agroforestry Activities in the Brazilian Amazon.

No. 10-09
Lu, D., E. Moran, and S. Hetrick. In Press. Detection of Impervious Surface Change with Multitemporal Remote Sensing Data in an Urban-rural Frontier.

No. 10-10
D. Lu, S. Hetrick, E. Moran, and G. Li. In Press. Detection of Urban Expansion with Multitemporal Quickbird Images. International Journal of Remote Sensing.

No. 10-11
Muehlenbein, M.P., J.L. Hirschtick, J.Z. Bonner, and A.M. Swartz. 2010. Toward quantifying the usage costs of human immunity: Altered metabolic rates and hormone levels during acute immune activation in men. American Journal of Human Biology 22: 546-556.

No. 10-12
Muehlenbein, M.P., L.A. Martinez, A.A. Lemke, L. Ambu, S. Nathan, S. Alsito, and R. Sakong. 2010. Unhealthy travelers present challenges to sustainable primate ecotourism. Travel Medicine and Infectious Disease 8: 169-175.

No. 10-13
Tucker, C.M. 2010. Private Goods and Common Property: Pottery Production in a Honduran Lenca Community. Human Organization 69(1): 43-53.

No. 10-14
Tucker, C.M., H. Eakin, and E.J. Castellanos. 2010. Perceptions of risk and adaptation: Coffee producers, market shocks, and extreme weather in Central America and Mexico. Global Environmental Change 20: 23-32.

No. 10-15
Lu, D., S. Hetrick, E. Moran, and G. Li. 2010. Detection of Urban Expansion in an Urban-rural Landscape with Multitemporal QuickBird Images. Journal of Applied Remote Sensing 4(041880): 1-17.

No. 10-16
Mattos, L., E. Brondizio, A. Romeiro, and R. Orair. 2010. Agricultural de pequena escala e suas implicações na transição agroecológica na Amazônia Brasileira. Amazônica 2(2): 220-248.